




# Radiofrequency applicator for biomass heating

Julián Corach, PhD<sup>1,2</sup>, Eriel Fernández Galván, Eng<sup>1</sup>, and Patricio Aníbal Sorichetti, PhD<sup>1</sup>

<sup>1,2</sup>Universidad de Buenos Aires, Argentina, jcorach@fi.uba.ar, fgalvan@fi.uba.ar, psorich@fi.uba.ar

<sup>3</sup>CONICET, Argentina

**Abstract**— *In electromagnetic biomass processing, which has gained academic and industrial interest in recent years, an electromagnetic field interacts with the biomass, heating it. Its applications include the defrosting, cooking and pasteurization of food, the disinfection of fruits, and the production of biofuels, among others. The main advantage of electromagnetic processing methods is that the heating takes place in the entire volume of the biomass to be treated; in addition, it has great flexibility for its application in batch or continuous processing, resulting in faster and efficient processes. Although applications at microwave frequencies have recently received more attention than the radio frequency range, the latter has an important advantage: as the operating frequency is lower, the radiation penetration depth is greater, allowing more uniform heating and the possibility of processing larger volumes. This work presents the design, construction and electrical characterization of an electromagnetic heating system suitable biomass processing. From reflection coefficient measurements between 1MHz and 30MHz, an equivalent electrical model is developed and its parameters are determined. The operation of the system is described, with emphasis on the applicator.*

**Keywords**—Radiofrequency heating, biomass, biodiesel, permittivity, transesterification.

## I. INTRODUCTION

In the last years, biomass products find renewed interest due to economic and environmental reasons. In the energy sector, fuels from biomass are seen as promising alternatives to conventional fossil fuels. In particular, biodiesel is a liquid fuel obtained from a transesterification reaction, in which a vegetable oil or an animal fat reacts with a short-chain alcohol, and a mixture of methyl esters and glycerol is obtained [1,2]. The reaction is carried out with continuous stirring, heating, and in the presence of a catalyst, such as sodium hydroxide or potassium hydroxide.

In Argentina, the industrial production of biodiesel is based on the use of soybean oil, methanol and sodium hydroxide as catalyst [3]. In most industrial scale plants, the heating process is based on the heat transfer from a hot surface to the volume of liquid. It is usually carried out with steam from boilers or conventional steam generators [4]. This process is inherently slow and inefficient. Therefore, it is interesting to speed up the process and reduce the energy consumption, both from the point of view of the production costs and also due to environmental concerns.

Electromagnetic heating techniques are based on the interaction between a time dependent electromagnetic field and the substance to be heated [5]. Contrarily to conventional heating process, during electromagnetic heating the interaction

between the fields and the substance takes place all over the volume to be heated, resulting in faster processes. These methods are usually referred to as “volumetric methods”. In industrial processes such as drying, sterilization, cooking, disinfection, etc. [5], volumetric heating techniques by radiofrequency and microwaves are extensively used.

It should be remarked that there are specific frequency bands reserved for industrial, scientific and medical applications (ISM bands), which are internationally regulated by the International Telecommunications Union (ITU) and correspond to frequencies between 6.765 MHz and 244 GHz. For example, the 2.45 GHz band is widely used in domestic microwave ovens.

In recent years, numerous researchers explored microwave heating during transesterification, to improve the efficiency of the reaction and to reduce the reaction time [6]. In many papers, the microwave energy is obtained using modified domestic ovens, so the operating frequency is 2.45GHz. In general, these works report experiments, at the laboratory, scale with very high conversion rates in very short times, compared to the standard heating methods [6]. However, the use of microwaves in large volumes (typical of the industrial scale) has limitations. Since the penetration depth of the waves at 2.45GHz is of the order of centimeters, the energy deposition would be limited to the outer regions of an industrial-scale reactor [5]. In addition, compared to radiofrequency systems, the implementation of high-power microwave heating systems in the industrial scale is more expensive and technically complex. In contrast, electromagnetic heating systems operating at the radiofrequency ISM bands (13.56 MHz, 27.12 MHz and 40.68 MHz), have comparative advantages for industrial scale applications. As the operation frequencies are lower, the depth of penetration is larger, in consequence they are more suitable for heating large volumes of liquids, allowing a more uniform heating [4,5,7,8]. In this regard, it is important to remark that, due to field inhomogeneity, hot-spots may appear causing a local temperature increase which may accelerate the reaction in an uncontrolled way [5]. Commercial radiofrequency heating and drying equipment are already available, with powers in the order of tens of kW [9]. They are widely used for drying, materials processing, disinfection, cooking food, waste water treatment, etc. [10,11].

Broadly speaking, radiofrequency heating systems consist of a radiofrequency generator, a power amplifier, an impedance matching system, and the applicator, which is the part of the system where the heating takes place. A typical system is schematized in Fig. 1. It should be remarked that in some commercially available systems, several blocks may be integrated in the same device, for instance, the power amplifier

**Digital Object Identifier:** (only for full papers, inserted by LACCEI).

**ISSN, ISBN:** (to be inserted by LACCEI).

**DO NOT REMOVE**

and the impedance matching system. Figure 1 also shows in more detail that the connection between the applicator and the matching system is usually implemented

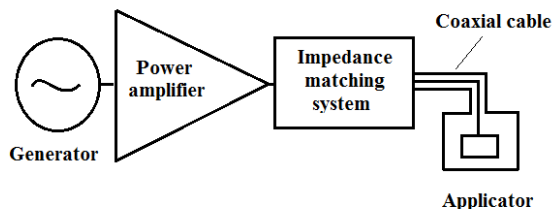


Fig. 1 Simplified scheme of a radiofrequency heating system.

with a coaxial cable. As it can be seen, the central conductor of the coaxial cable is connected to a metallic (active or “hot”) electrode inside the applicator, and the outer conductor is connected to the body of the applicator (also metallic).

Clearly, one of the key elements of the heating system is the applicator, since it is where the heating takes place. It should have low electromagnetic losses, an adequate input impedance, low inductance, and, preferably, it should have no resonances in the frequency range of operation. Also, its construction must be robust and with materials carefully chosen, to avoid deformations, oxidation, chemical attack, etc. It is important that to remark that, although many papers deal with radiofrequency and microwave heating systems, there is comparatively less information on electromagnetic applicators. Therefore, this paper describes the design, construction, and electrical characterization of a laboratory electromagnetic applicator operating at 13.56 MHz and 27.12 MHz.

## II. DESIGN AND CONSTRUCTION

The electromagnetic heating system (EHS) used in this work is schematized in Fig. 1. The generator produces low power signals (of the order of mW) with low harmonic content, which are amplified to powers in the order of tens of W. The reflection of power between the different parts of the system must be minimized since they may damage the equipment, so all components should be matched to the output impedance of the generator and the amplifier (50  $\Omega$ , in this work). The impedance matching can be achieved with automatic commercial equipment, or with manually controlled combinations of variable inductors and capacitors. In this work, an automatic impedance matching system was used for this purpose.

Fig. 2 shows photographs of the different parts of the applicator, which is based on a cylindrical structure. In the base of the applicator (Fig. 2 A) there are two circular clefts where PMMA tubes, used as a vessels, may be locked in place; this allows to select two different operating sample volumes. The cylindrical walls of the metallic body are press-fitted in the base, ensuring good electrical contact between them. The

lid of the applicator (Fig. 2 B) is a circular metallic plate. The active electrode is held in place with PMMA spacers.

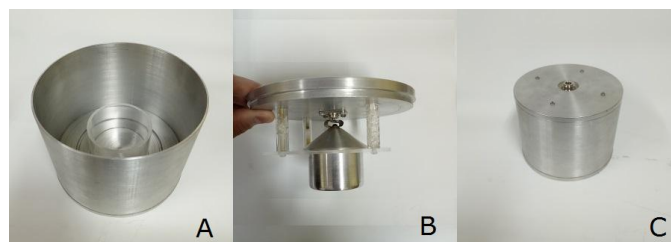


Fig. 2 Photographs of the applicator.

The active electrode was mechanized from a solid aluminum cylinder. Its upper part is conical in order to reduce parasitic capacitances and inductances, to avoid sharp edges, and to reduce its weight. The lower part of this electrode is cylindrical, with the lower edges rounded (again, to avoid sharp edges). The upper part of the cone is attached to a very short length of copper foil, that is soldered to the central pin of an N-type female panel radio frequency connector (Amphenol model 82-97-RFX). This connector has very low losses, and is held in place to the lid with screws. In this way, the base, the walls, the lid and the outer connector part are electrically connected.

When the lid is placed on the body of the applicator, the lower part of the active electrode and the base of the applicator form a parallel planar capacitor. The lid also has a recess in its edge, which allows it to be press fitted to the body of the applicator with good electrical contact.

The metallic parts material was chosen according to compatibility requirements. To prevent the chemical attack on the metals during transesterification, stainless steel or aluminum can be used in all parts that are in contact with the substances to be processed. For reasons of cost, weight, and ease of machining reasons, aluminum was chosen in this work. However, in future designs, the use of stainless steel is expected, given its better durability and broader range of compatibility. As explained above, two PMMA tubes may be used, with internal diameters of 6.5 cm and 9.5 cm. Therefore, the volume of material in the applicator ranges from less than 0.1 L to more than 0.2 L, depending on the height of the sample to be heated.

A cutaway drawing of the applicator is shown in Fig. 3.

As indicated above, during transesterification, the mixture of vegetable oil, alcohol, and catalyst must be continuously stirred. For this purpose, the applicator is placed on a magnetic stirrer and a magnetic mixer bar is submerged in the sample. It is important to note that the metal used for the base of the applicator must be paramagnetic (such as aluminum), so that the magnetic field lines pass through it, and the magnetic stirrer bar rotate with an adequate speed.

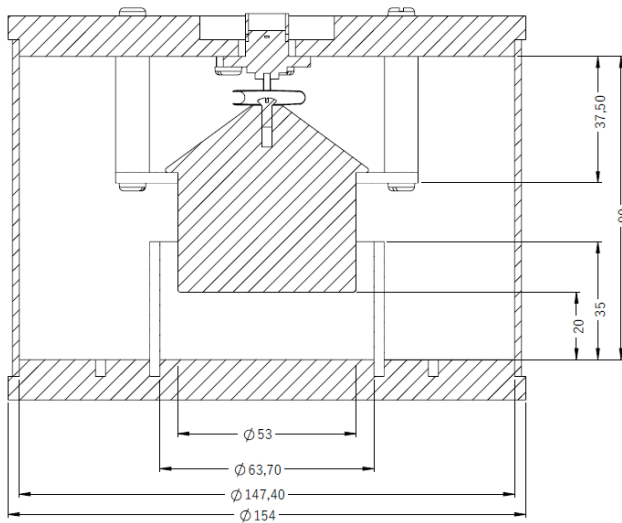


Fig. 3 Cutaway drawing of the applicator.

The active region of the applicator is the volume in which the sample to be treated is placed. It is formed by the space between the lower part of the active electrode, and the base of the applicator. The volume of sample subjected to the electric field is then determined by the distance between the area of the lower part of active electrode and the base of the applicator, and by the diameter of the PMMA tube used to contain laterally the sample. It is important to note that, for the electric field to concentrate in the active region, the capacitance between the active electrode and the other parts of the applicator must be minimized.

As a first approximation, neglecting parasitic effects, the capacitance  $C_o$  of the active part the applicator, when empty, can be estimated as:

$$C_o = \epsilon_o A / d \quad (1)$$

where  $A$  is the area of the lower part of the active electrode,  $d$  is the distance between it and the base of the applicator, and  $\epsilon_o$  is the vacuum permittivity ( $8.8541 \times 10^{-12}$  F/m). It is important to note that the total capacitance of the applicator will also include the parasitic capacitances between the active electrode and all the other metallic parts.

### III. ELECTRICAL CHARACTERIZATION

To experimentally determine the value of  $C_o$ , measurements of the "cable + applicator" system were carried out between 1 MHz and 1GHz using a vector impedance measuring system (VNA) outlined in Figure 4.

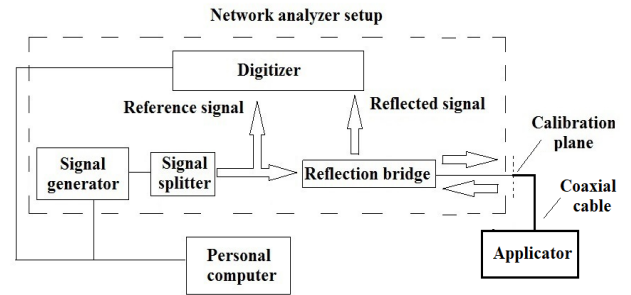


Fig. 4 VNA measurement system.

The vector network analyzer setup consists of a signal generator (HP 8648A), a two-channel digital sampling oscilloscope (Agilent Infinium), a microwave splitter (Agilent 11667A), and a directional bridge HP 86205A (300 kHz - 6 GHz). The signal from the generator is split into a reference signal, which is directly digitized by one of the channels of the oscilloscope, and an excitation signal that reaches the sample under test through the reflection bridge. A portion of the signal reflected by the sample, is captured by the second channel of the oscilloscope through the reflected port of the directional coupler. The digitized signal were processed by an FFT routine in a PC to obtain the complex reflection coefficient. The excitation frequency was swept between 1 MHz and 1 GHz, in 5 MHz steps. More details about the measuring system are given in [12].

Prior to measurements, to reduce systematic errors, a short-open-load (SOL) calibration was performed at the calibration plane (see Figure 1) with an Agilent 85032E type N kit. The applicator was connected to the reflection bridge through a 20 cm low loss coaxial cable with N connectors in both ends. With this system, the complex reflection coefficient,  $\rho(\omega)$ , was determined in magnitude and phase as a function of the frequency. The operation of the measurement system is described in detail in [12].

Figs. 5 and 6 show the reflection coefficient of the empty applicator between 1 MHz and 1 GHz, in magnitude and phase respectively.

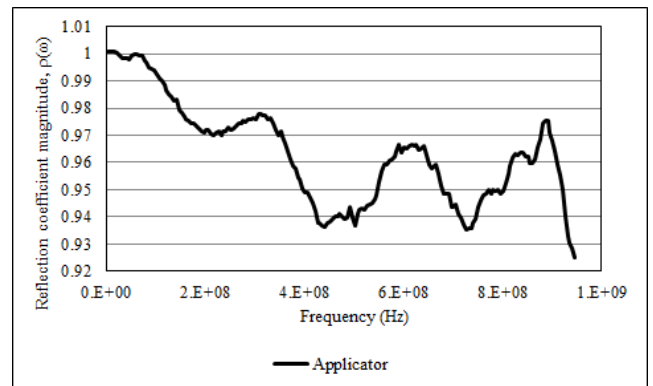


Fig. 5 Reflection coefficient magnitude between 1 MHz and 1 GHz.

From Fig. 5, it can be seen that the electrical losses of the applicator are lower than 3% up to approximately 280 MHz, and lower than 8% up to 1 GHz. Although losses increase at higher frequencies, the applicator is not intended to be used in those frequency ranges.

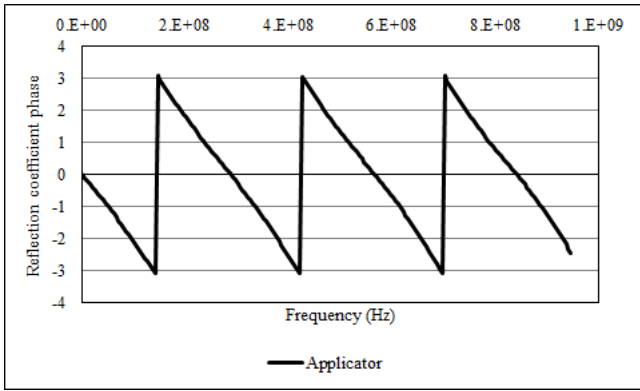


Fig. 6 Reflection coefficient modulus between 1 MHz and 1 GHz.

From Fig. 6, it can be seen that the phase of the reflection coefficient of the applicator is nearly linear with frequency.

From the reflection coefficient measurements, it is possible to calculate the equivalent admittance,  $Y(\omega)$ , as:

$$Y(\omega) = 1/Z_0(1 - \rho(\omega))/(1 + \rho(\omega)) \quad (2)$$

where  $Z_0$  is the characteristic impedance of the system (in this case 50 Ohm). Figures 7 and 8 show the magnitude and phase of  $Y(\omega)$  up to 1 GHz. The results presented in Figs. 5 to 8 are very important since they show that the first resonance (series resonance) takes place at around 140 MHz, that is a frequency much higher than the intended operating frequencies (13.56 MHz and 27.12 MHz).

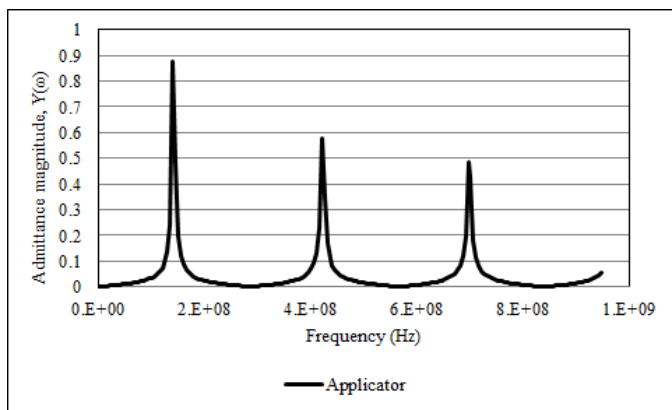


Fig. 7 Magnitude of the admittance between 1 MHz and 1 GHz.

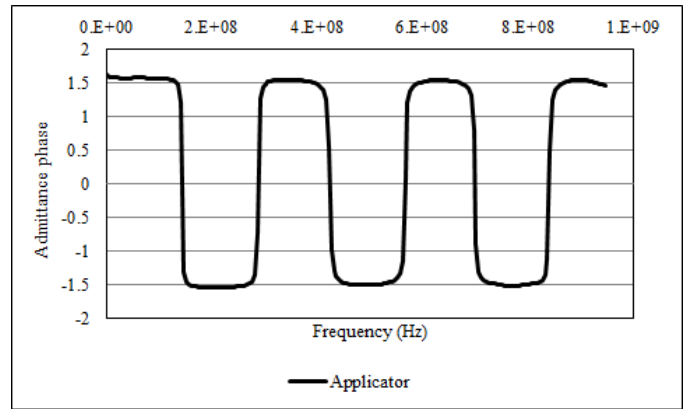


Fig. 8 Admittance phase between 1 MHz and 1 GHz.

Since the changes in the phase of the admittance at the resonances are very sharp, as shown in Fig. 8, it is easy to see that the losses are very low, even at high frequencies. It is important to remark that, to measurements presented in Figs. 5 to 8 include the effect of the coaxial cable used for the connection of the applicator to the measuring system. This means that the first resonance of the applicator is even higher than 140 MHz. However, since the applicator must be connected to the power amplifier by a short length of coaxial cable, it is important to verify the resonance of the system including the cable. However, in order to properly characterize the applicator and to determine its parameters, the effect of the coaxial cable will be considered during the analysis.

The magnitude and phase of the reflection coefficient of the empty applicator between 1 MHz and 30 MHz are shown in detail in Figs. 9 and 10 respectively (circles); the results for the applicator with a sample of very low conductivity deionized water (triangles), are also shown.

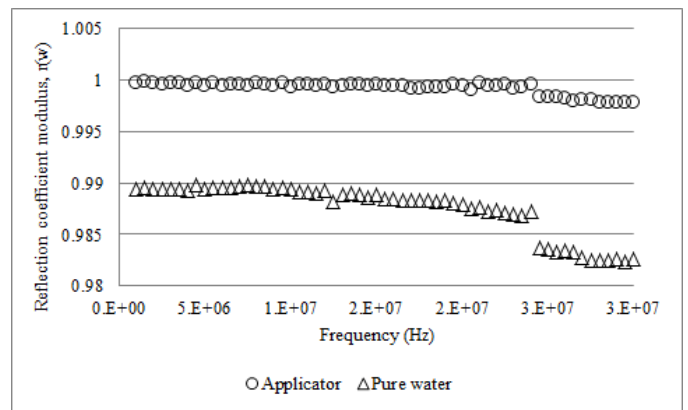


Fig. 9 Reflection coefficient modulus between 1 MHz and 30 MHz.

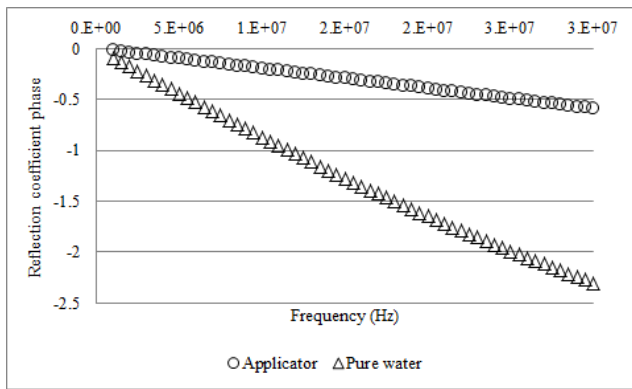


Fig. 10 Reflection coefficient phase between 1 MHz and 30 MHz.

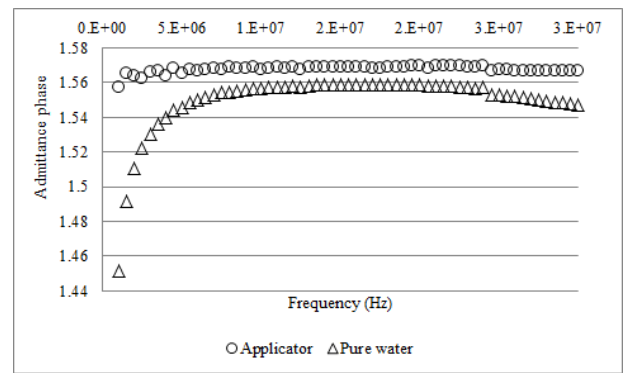


Fig. 12 Admittance phase between 1 MHz and 30 MHz.

In Fig. 9 it can be seen that losses increase slightly when a sample of water with very low conductivity is introduced in the applicator (the magnitude of  $\rho(\omega)$  is very close to 1).

Figs. 11 and 12 show, respectively, the magnitude and phase of the admittance of the empty applicator in air, and with a low conductivity water sample between 1 MHz and 30 MHz. From Fig. 10, it is clear that a parasitic inductive effect must be considered for modeling purposes. Also, from Fig. 11 it can be seen that the applicator with water has slightly higher losses than in air.

For design and simulation purposes it is very important to develop a model of the applicator, and to accurately determine its parameters. The coaxial cable used for the connection of the applicator has very low losses, and be therefore modeled as an ideal (lossless) transmission line. For the modeling of the applicator, up to 30 MHz, lumped elements are used.

Ideally, the applicator should be a capacitor. If so, the magnitude of the admittance would increase linearly with frequency, and its phase would be exactly  $\pi/2$ . However, from the experimental results, it is seen that parasitic effects must be considered. To model the electrical losses, a resistor is connected in parallel with the capacitor. Also, due to parasitic inductive effects (see Fig. 7), the magnitude of the admittance increases with frequency more rapidly than in a pure capacitive. In consequence, the model includes an inductor in series with the capacitor.

From the above, the circuit shown in Fig. 13 is proposed to model the coaxial cable and the applicator; the measuring plane of the input admittance  $Y(\omega)$  is also indicated.

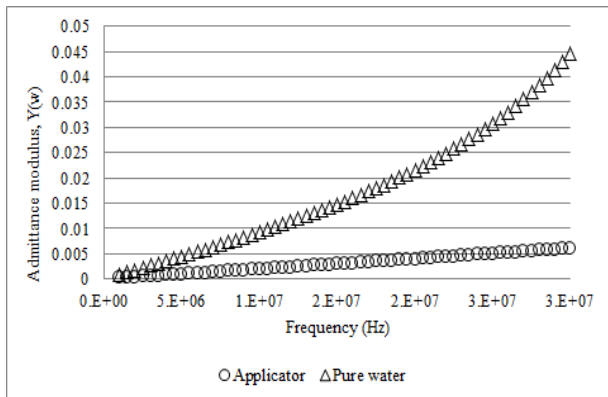


Fig. 11 Admittance modulus between 1 MHz and 30 MHz.

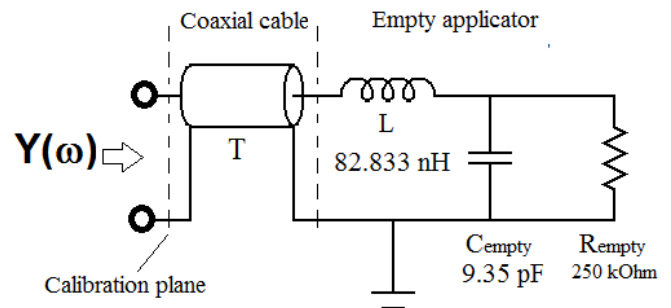


Fig. 13 Equivalent circuit of the empty applicator.

The determination of the value of each parameter (indicated in Fig. 13) was carried out with specialized software Microcap12 [13], freely available. The values were fitted to the values of the complex admittance  $Y(\omega)$ .

The coaxial cable (T) was previously measured to determine its characteristic impedance and the propagation delay. The fitted values were  $55.75 \Omega$  and  $1.089 \text{ ns}$ .

The applicator is modeled by lumped circuit elements (L, C and R). The parasitic inductive effects are represented by the inductance L, and are mainly due to the length of the active electrode, and by the short pin of the N-type connector;  $C_{\text{empty}}$

includes the capacitances of the N-type connector, parasitic capacitances, and the active part capacitance; finally,  $R_{empty}$  represents the applicator losses, and, since these are very low, the value of the resistor is very high.

One of the most important design parameters of the applicator is the value of the capacitance of the active part, which is formed between the active electrode and the base of the applicator; this capacitance is indicated as the active capacitance,  $C_o$ , and the capacitances of all the other parts are referred to as parasitic capacitances,  $C_p$ . When the applicator is empty, the value of the capacitance includes both the active and parasitic capacitances. If a sample is placed in the active region, a change in the total capacitance is found, and is due only to the presence of the sample. Therefore, to separate the active and parasitic capacitances, two measurements must be made: one with the empty applicator, and a second one with the applicator filled with a sample of well-known electrical properties [14,15]. We used pure water of very low conductivity as a reference liquid. The capacitance of the empty applicator,  $C_{empty}$ , can be written as

$$C_{empty} = C_o + C_p \quad (3)$$

When the sample of low conductivity water is introduced in the active region, the total capacitance of the applicator,  $C_{total}$ , is

$$C_{water} = C_o \epsilon_r + C_p \quad (4)$$

where  $\epsilon_r$  is the relative permittivity of the sample. The difference between  $C_{water}$  and  $C_{empty}$ ,  $\Delta C$ , is

$$\Delta C = C_o (\epsilon_r - 1) \quad (5)$$

where  $\epsilon_r$  is the low-frequency value of the permittivity of pure water [14,15].

Figure 14 shows the equivalent circuit of the applicator with low conductivity water, together with the fitted values. As it can be seen, the value of the inductance,  $L$ , does not change. The value of the capacitance of the applicator with low conductivity water,  $C_{water}$ , is higher, and that of the empty applicator, and the value of the resistor is lower (because the losses of the applicator with water, although very low, are higher than those of the empty applicator).

The value of  $C_o$  from the fitted experimental data is 1.25 pF. This is fairly close to the value of an ideal plane parallel capacitor with electrode of area  $A$  and separation  $d$  (see (1)). Of course, this simple model cannot take into account the geometry of the applicator shown in Fig. 3. For instance, in this model, edge effects are neglected and the details of the rounded edge in the active electrode are ignored. Moreover, the geometric volume of the active region, defined by the surface area of lower part of the electrode and the distance of the electrode,  $(Ad)$ , is 60 mL.

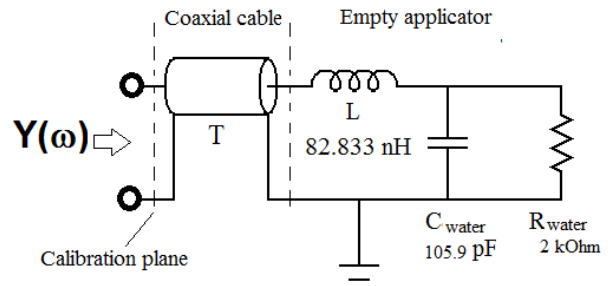


Fig. 14 Equivalent circuit of the applicator with water.

In order to assure good contact between the lower part of the active electrode and the sample, the sample volume loaded into the holder of the applicator is 70 mL (that volume is accurately determined using a precision pipette). Therefore, a part of the active electrode is partially submerged into the sample. In consequence, neglecting border effects is not an appropriate simplification.

As mentioned above, for the production of biodiesel, a vegetable oil (with relative permittivity around 3) is mixed with methanol (with relative permittivity around 33). The permittivity of oil-methanol mixtures is then expected to have an intermediate value between 3 and 33. Even if pure methanol was used, the total capacitance value would be less than 100 pF. These values are adequate for commercially available impedance matching systems.

#### IV. CONCLUSIONS

This paper presents the design, construction and electrical characterization of an electromagnetic applicator for biomass processing with radiofrequency heating. Design criteria and material selection is discussed in detail. The electrical characterization of the applicator is carried out analyzing experimental results of the reflection coefficient between 1 MHz and 1 GHz. From experimental data, a model of the applicator is developed, and its parameters are determined from fitting to experimental data. From the experimental results, it is verified that the applicator has very low losses in the frequency range of interest, a key point for efficient heating. Also, from the model analysis, it is confirmed that the inductance is very low, and that the first electrical resonance takes place at frequencies well above the operating range. The electrical characterization of the applicator is a key part of the overall performance of the complete system fundamental requirement for the correct selection of the impedance matching system.

#### ACKNOWLEDGMENT

This work was supported with Projects PICT 2019 N° 1076 and PICT 2020 A N° 3741, from FONCyT, and

## REFERENCES

- [1] G. Knothe, J. Krahl, J. Van Gerpen. "The Biodiesel Handbook". 2<sup>nd</sup> ed., Urbana: AOCS Press, 2010.
- [2] SD. Romano, PA. Sorichetti. Dielectric relaxation spectroscopy in biodiesel production and characterization, London: Springer Verlag, 2011.
- [3] Informe Secretaría de Energía de la Nación. [https://www.agroindustria.gob.ar/sitio/areas/bioenergia/informes/\\_archivos/000003\\_Informes%20Biocombustibles%202019/190400\\_Informe%20Biocombustibles%20\(Abril%202019\).pdf](https://www.agroindustria.gob.ar/sitio/areas/bioenergia/informes/_archivos/000003_Informes%20Biocombustibles%202019/190400_Informe%20Biocombustibles%20(Abril%202019).pdf)
- [4] M. Tabatabaei, M. Aghbashlo, M. Dehghani, HKS. Panahi, A. Mollahosseini, M. Hosseini, MM. Soufiyan. "Reactor technologies for biodiesel production and processing: A review", *Progress in Energy and Combustion Science* 2019;74:239-303.
- [5] GB. Awuah, HS. Ramaswamy, J. Tang. "Radio-Frequency Heating in Food Processing", London: CRC Press, 2015.
- [6] JJ. Lin, YW. Chen. "Production of biodiesel by transesterification of Jatropha oil with microwave heating", *J Taiwan Inst Chem Eng*, 75, pp. 43–50, 2017.
- [7] S. Liu, Y. Wang, T. McDonald, SE. Taylor. "Efficient production of biodiesel using radio frequency heating", *Energy & Fuels*, vol. 22, pp. 2116-2120, 2008.
- [8] S. Liu, Y. Wang, JL. Herring. "Fast biodiesel production from beef tallow with radio frequency heating". *Renewable Energy*, vol. 36, pp. 1003-1007, 2011.
- [9] <https://radiofrequency.com/general-industry/>
- [10] S. Wang, J. Tang. "Radio frequency and microwave alternative treatments for insect control in nuts: a review". *Int Agric Eng J*, vol. 10, pp. 105–120, 2001.
- [11] MC. Lagunas-Solar, JS. Cullor, NX. Zeng, TD. Truong, TK. Essert, WL. Smith, et al. "Disinfection of dairy and animal farm wastewater with radiofrequency power". *J Dairy Sci*, vol. 88(11), pp. 4120–4131, 2005.
- [12] J. Corach, E. Galván Fernández, PA. Sorichetti, SD. Romano. "Broadband permittivity sensor for biodiesel and blends". *Fuel* 254, 2019. <https://doi.org/10.1016/j.fuel.2019.115679>
- [13] Microcap 12. <http://www.spectrum-soft.com/index.shtm>
- [14] AP. Gregory, RN Clarke. "Traceable measurements of the static permittivity of dielectric reference liquids over the temperature range 5–50°C". *Meas Sci Technol*, vol. 16, pp. 1506–16, 2005.
- [15] A. Stogryn. "Equations for calculating the dielectric constant of saline water" (correspondence). *Microwave Theory and Techniques, IEEE Transactions*, vol. 19, pp. 733-736, 1971.